Supporting Information For

Factors Governing the Chemical Stability of Shear-Exfoliated ZnSe(alkylamine) II-VI Layered Hybrids

Mengwen Yan,[1] Sean M. Collins,[2,3] Paul A. Midgley,[3] Jeremy I. Feldblyum[1]*

Equation S1.

Stokes' Law[1]:

$$v = \frac{2R^2}{9\mu}(\rho_P - \rho_L) \times g$$

where v is the sedimentation velocity for spherical particles, R is particle's radius, μ is the liquid medium viscosity, ρ_P and ρ_L are the particle and the liquid medium density, respectively, and g is the acceleration due to gravity.

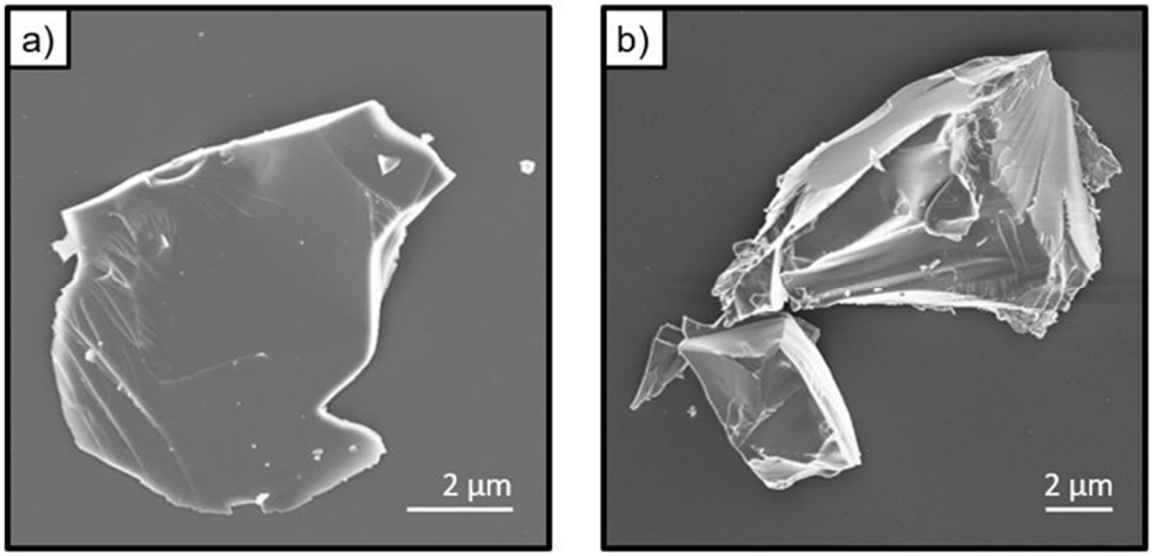

Figure S1. SEM image of bulk (non-exfoliated) a) ZnSe(ba) and b) ZnSe(oa).

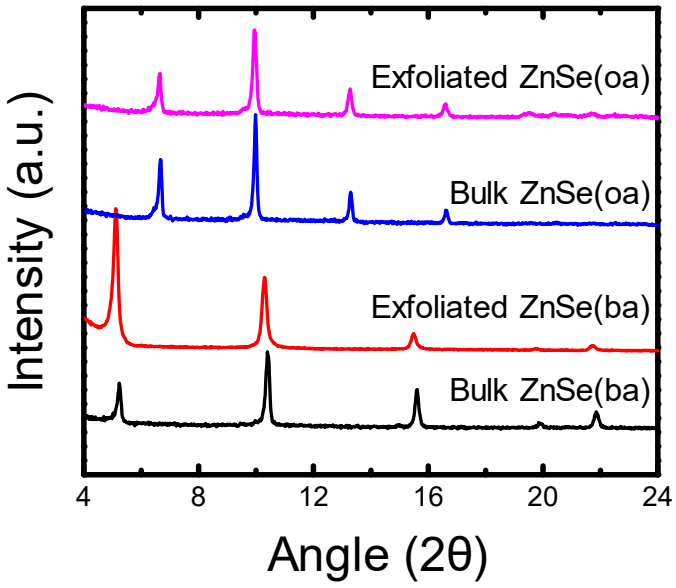

Figure S2. Powder X-ray diffractograms of ZnSe(ba) and ZnSe(oa) before and after exfoliation from EtOH.

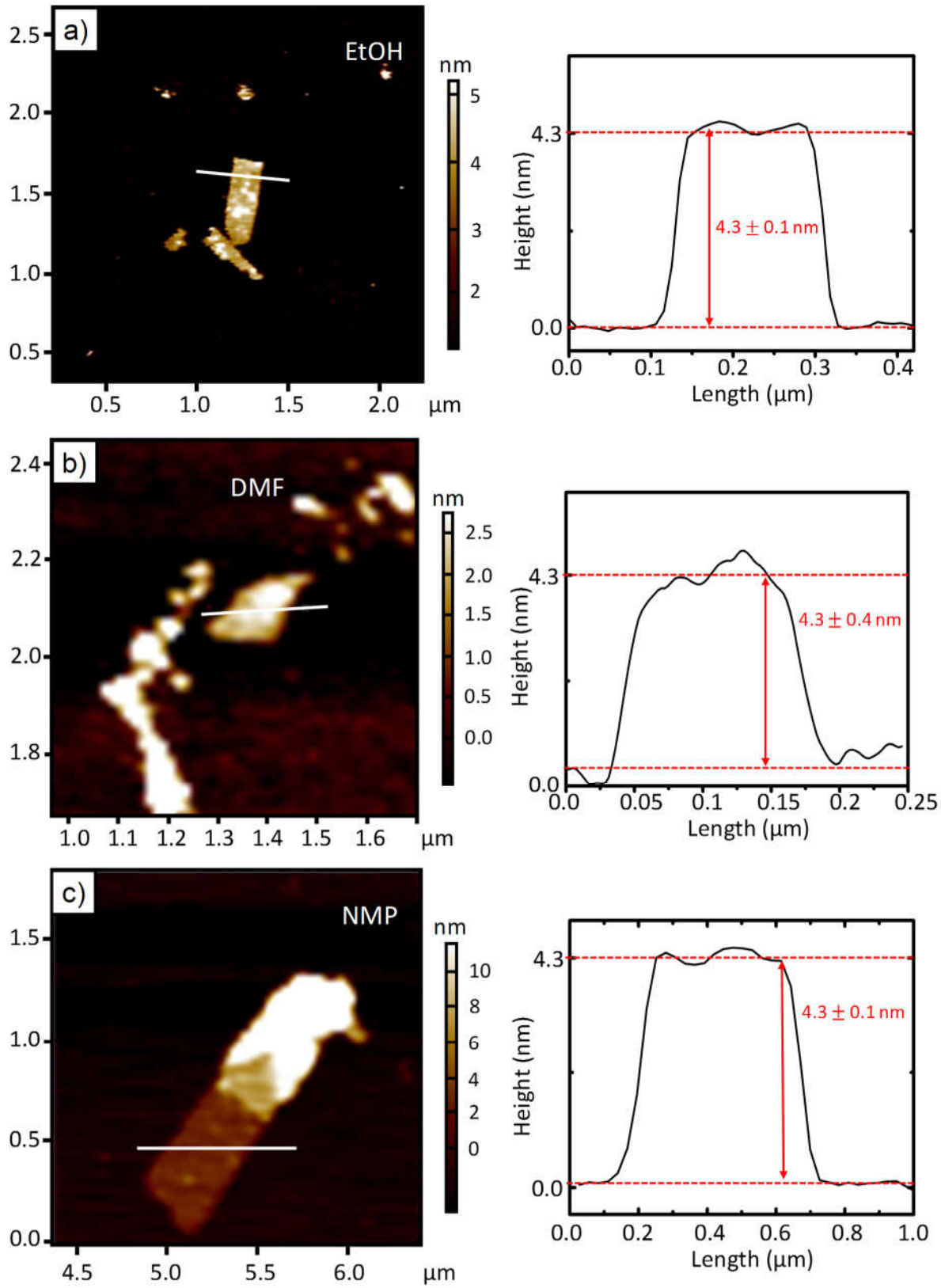
a)
EtOH
nm
5
4
3
2
2.5
2.0
1.5
1.0
0.5
0.5
1.0
1.5
2.0
µm
4.3
0.0
Height (nm)
4.3 ± 0.1 nm
0.0
0.1
0.2
0.3
0.4
Length (µm)
b)
DMF
nm
2.5
2.0
1.5
1.0
0.5
0.0
2.4
2.2
2.0
1.8
1.0
1.1
1.2
1.3
1.4
1.5
1.6
µm
4.3
0.0
Height (nm)
4.3 ± 0.4 nm
0.0
0.05
0.1
0.15
0.2
0.25
Length (µm)
c)
NMP
nm
10
8
6
4
2
0
1.5
1.0
0.5
0.0
4.5
5.0
5.5
6.0
µm
4.3
0.0
Height (nm)
4.3 ± 0.1 nm
0.0
0.2
0.4
0.6
0.8
1.0
Length (µm)

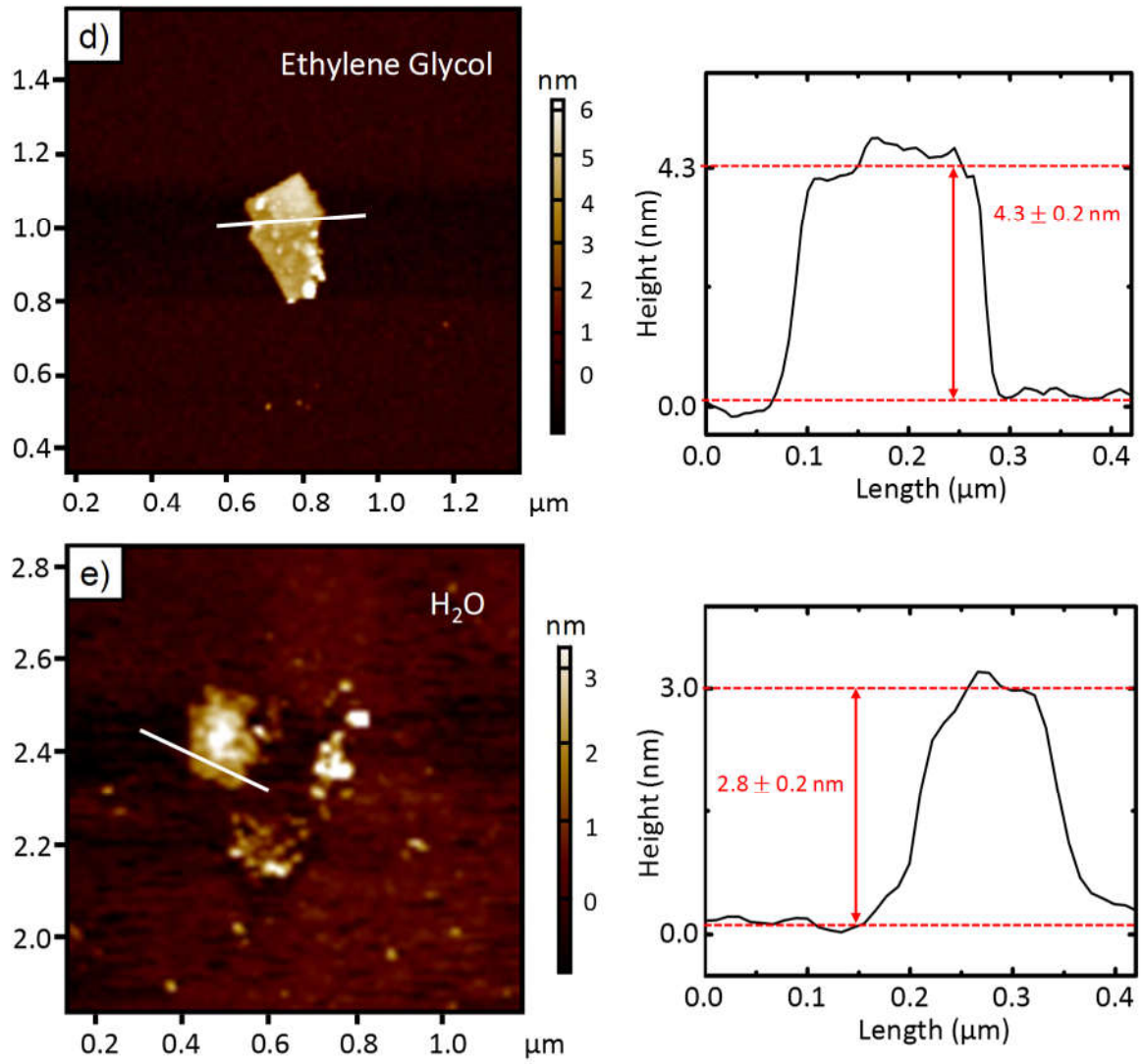

Figure S3. Tapping mode AFM data and height measurements of representative thinnest flakes of ZnSe(ba) exfoliated from different solvents. a) EtOH; b) DMF; c) NMP; d) ethylene glycol; e) H_2O.

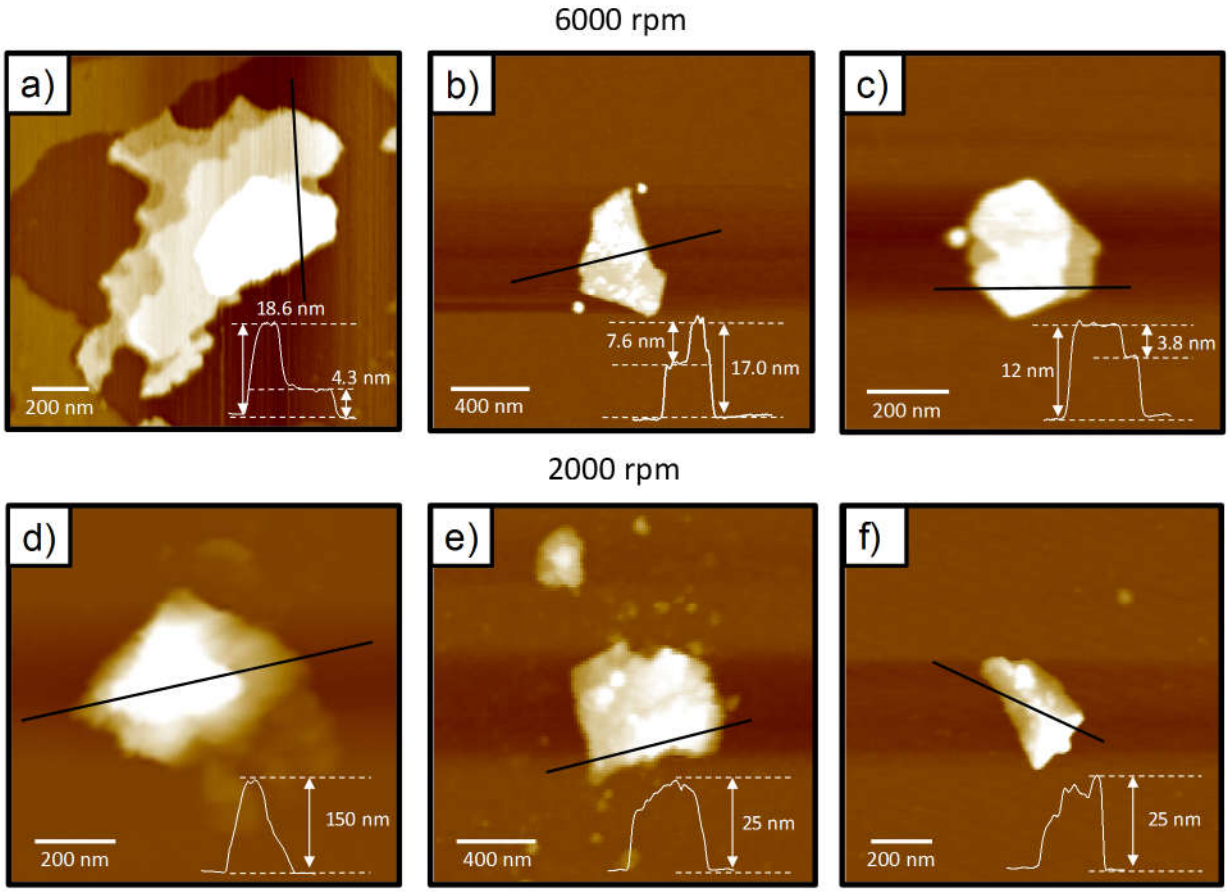

Figure S4. AFM images of typical ZnSe(ba) flakes exfoliated in EtOH at 6000 rpm (a-c) or 2000 rpm (d-f) for 1 h.

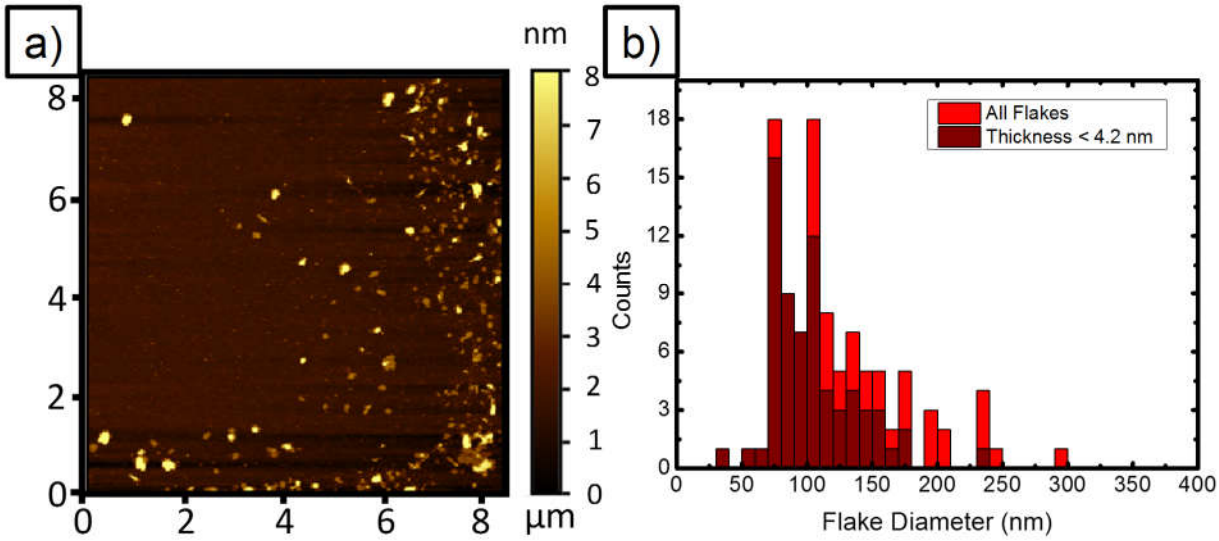

Figure S5. a) Wide field AFM image of ZnSe(ba) exfoliated from EtOH at 6000 rpm for 1 h. b) Diameter distribution of flakes in panel (a) determined by image analysis. Diameters of all flakes (red) and those having thickness < 4.2 nm (corresponding to bilayer material, dark red) are shown.

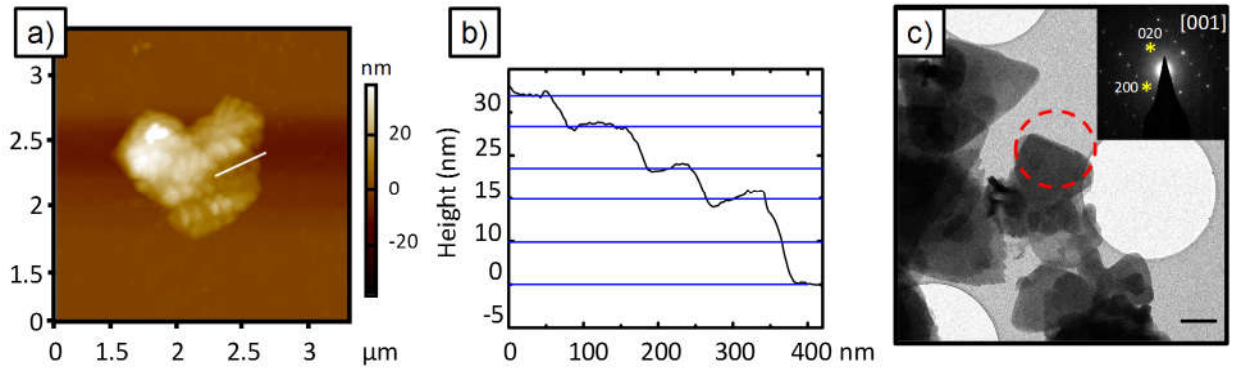

Figure S6. a) AFM image of ZnSe(oa) exfoliated from EtOH. The white line corresponds to step height measurement in panel (b). b) Step height of multilayer flake shown in panel (a). c) TEM image of ZnSe(oa) exfoliated from EtOH (scale bar: 500 nm) and corresponding SAED pattern (inset) viewed along the [001] zone axis for the region marked by a dashed red circle.

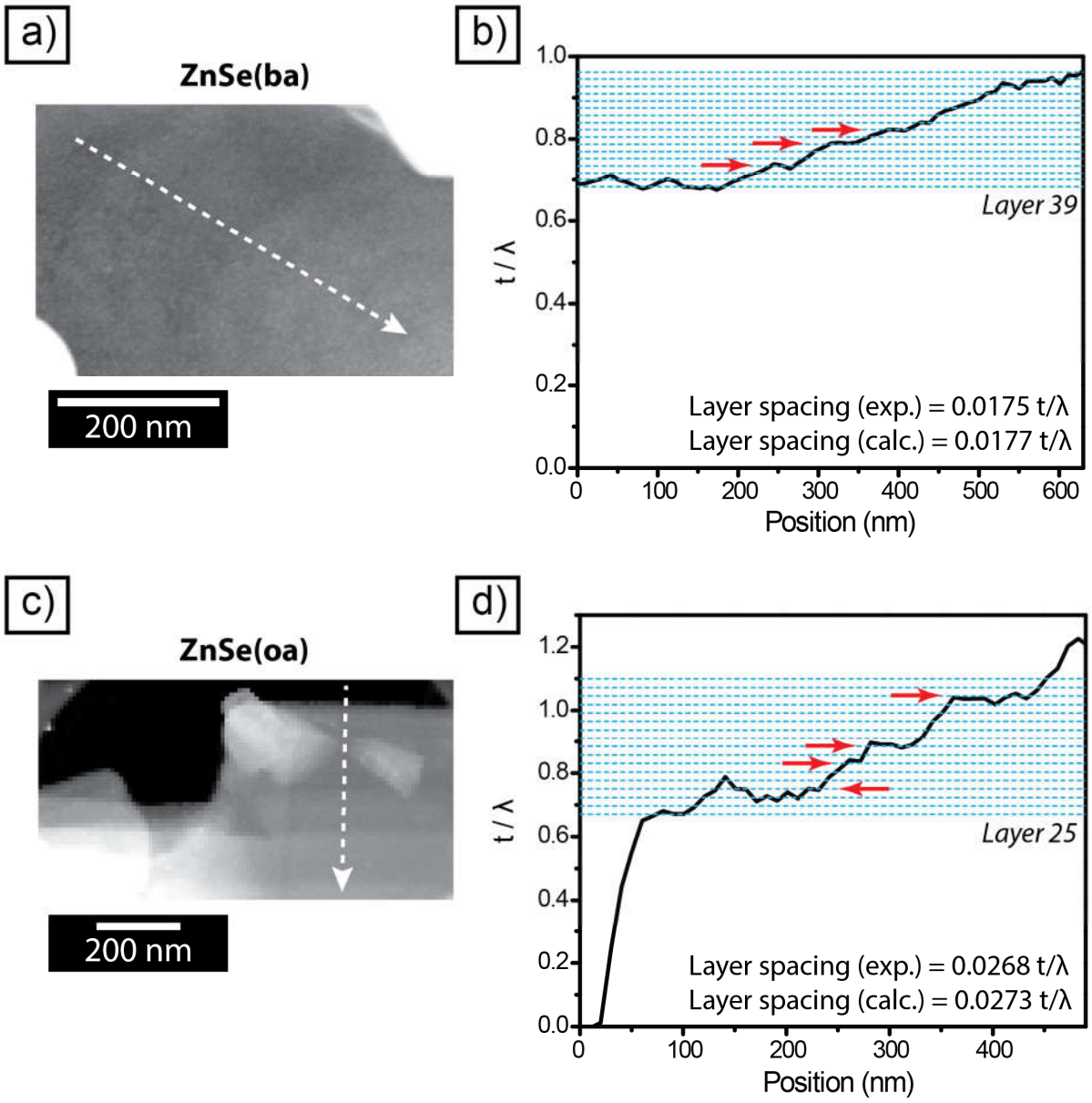

Figure S7. Layer thickness analysis for a)-b) ZnSe(ba) and c)-d) ZnSe(oa) based on electron energy loss spectroscopy (EELS) data using the ratio of the thickness (t) and mean free path for inelastic electron scattering (λ). Annular dark field STEM micrographs are shown in a) and c) for reference. The white dashed arrow indicates the location of the line profile used for EELS analysis, corresponding to the black line traces across series of steps in b) and d). Light blue dashed lines indicate unit layer step heights. Red arrows highlight key step positions in agreement with the light blue lines. Further information is provided below.

Measurement of Layer Thickness by EELS

Figure S7 presents an analysis of the layer thickness in ZnSe(ba) and ZnSe(oa) based on EELS data. The elastic scattering and total scattering signals recorded in EELS enable the determination of the ratio t/λ based on the expression:[2]

$$\frac{t}{\lambda} = \ln\left(\frac{I_t}{I_0}\right)$$

where I_t is the integrated area of the entire energy loss spectrum including the zero loss peak (ZLP) and I_0 is the area under the ZLP (the elastic scattering).

This unitless ratio provides a relative thickness measurement which in turn enables absolute thickness determination for a known value of the inelastic mean free path λ. Here, λ was calculated following the method proposed by Iakoubovksii et al.[3] which is parameterized by the density of the material and the electron optical configuration only. We have used the calculated density to calculate λ and used this to determine the expected interlayer t/λ. As noted on the figure, this calculation gave values for t/λ of 0.0175 for ZnSe(ba) and 0.0273 for ZnSe(oa). These estimates were refined against experimental data by adjusting this parameter to fit the steps observed in traces of experimental t/λ data.

In Figure S7, the experimentally refined values match the changes in thickness between not only major steps but most local thickness fluctuations, showing high quality agreement with the calculated thickness values.

This analysis corroborates layer step measurements recorded in AFM and provides clear evidence of the expected difference in layer spacing for butylamine- and octylamine-exfoliated ZnSe(alkylamine) materials.

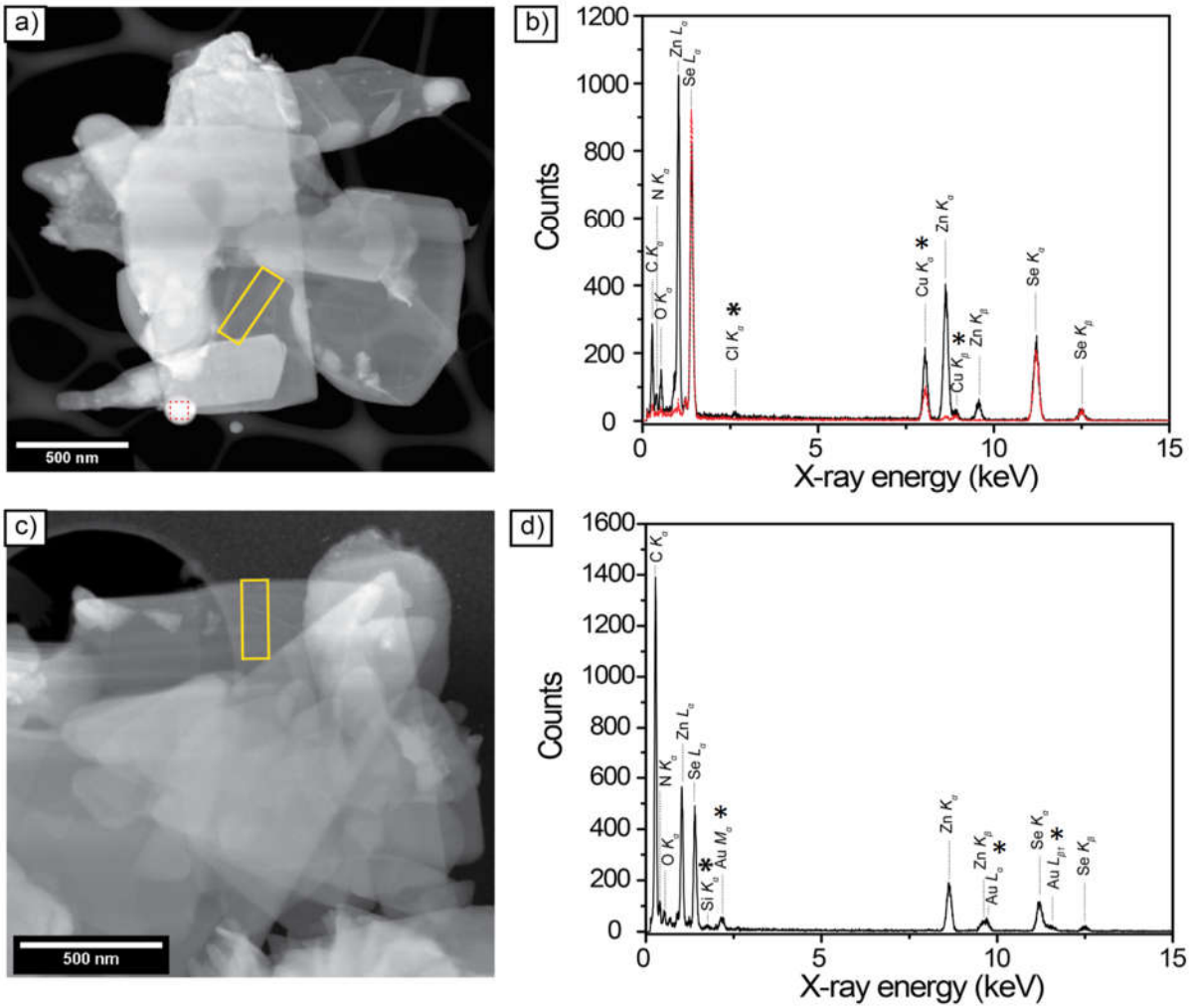

Figure S8. a, c) ADF-STEM and b, d) X-ray EDS selected area spectra for (top) ZnSe(ba) and (bottom) ZnSe(oa) exfoliated with EtOH. The yellow rectangle marks the location of the acquired spectrum (black). A red dashed square marks the location from which a second spectrum was acquired. We attribute this feature, a spheroid particle approximately 50 nm in diameter, to sample degradation. Cu and Au peaks result from the TEM grid substrates. The carbon support film contributes C and O signals. Signals attributed solely to the TEM grid material (Cu and Au) or trace contamination of the grid, support film, or sample in the form of Cl and Si are annotated with asterisks.

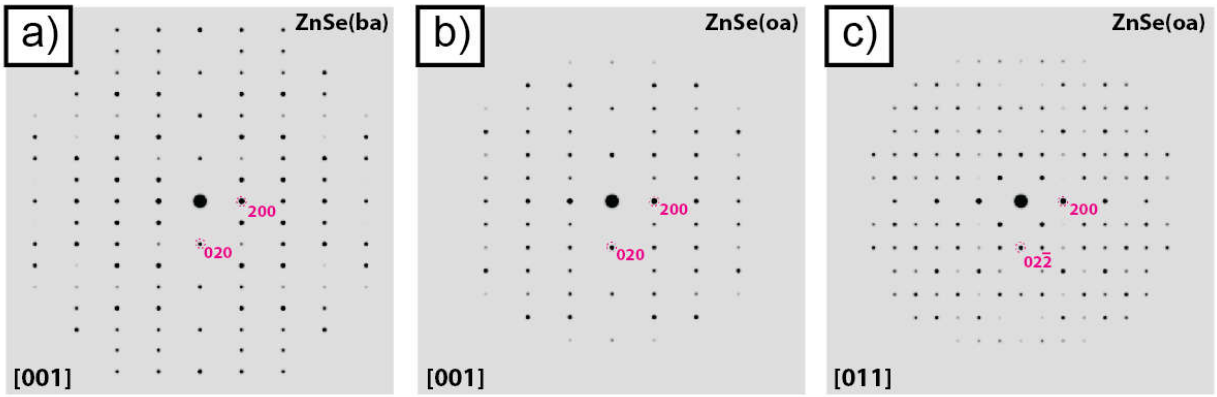

Figure S9. Kinematical electron diffraction patterns simulated for a) ZnSe(ba) and b)-c) ZnSe(oa) at 200 kV. Key reflections are labeled in pink and the orientation is defined relative to the beam direction as indicated in the lower left corner of each pattern. Both [001] and [011] patterns are shown for ZnSe(oa) given the appearance of 111 reflections in experimental scanning electron diffraction (SED) data. The pattern symmetry and intensities match experimental patterns well. In some experimental SED data on ZnSe(oa) (Figures 5 and S19), 111 type reflections are also observed, consistent with a small tilt of the crystal relative to the [001] zone axis. Due to the large real space interlayer distance in ZnSe(oa), which is therefore a very short distance in reciprocal space, even a very small tilt of a thin crystal with elongated reciprocal 'rods' in the direction normal to the flake surface will result in the appearance of reflections observed in the simulated [011] zone axis pattern. Facets are indexed based on the [001] patterns which correspond to the lowest order facets which can be reasonably assigned and which also match the selected area electron diffraction patterns (Figure 2f).

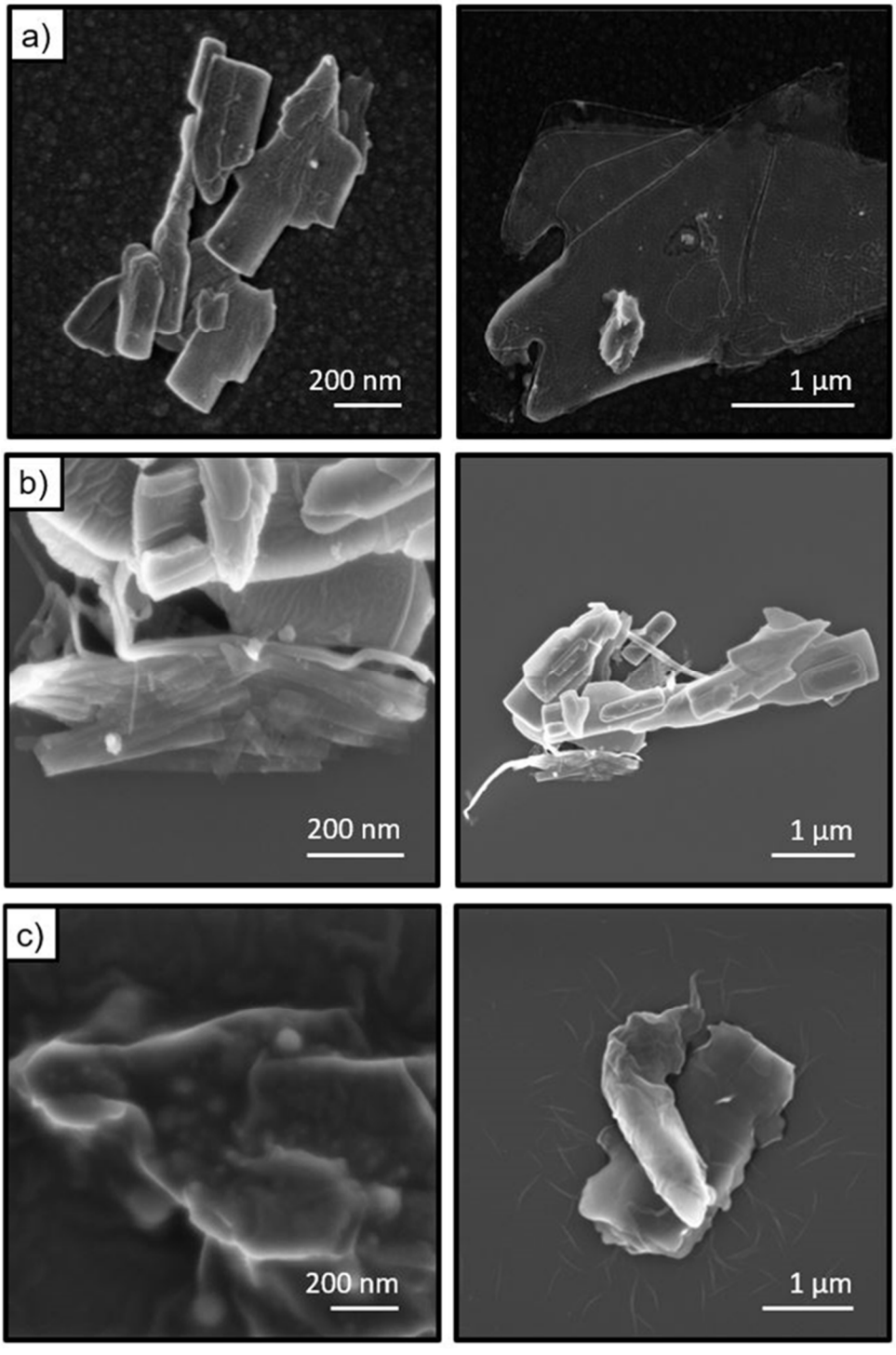
a)
200 nm
1 µm
b)
200 nm
1 µm
c)
200 nm
1 µm

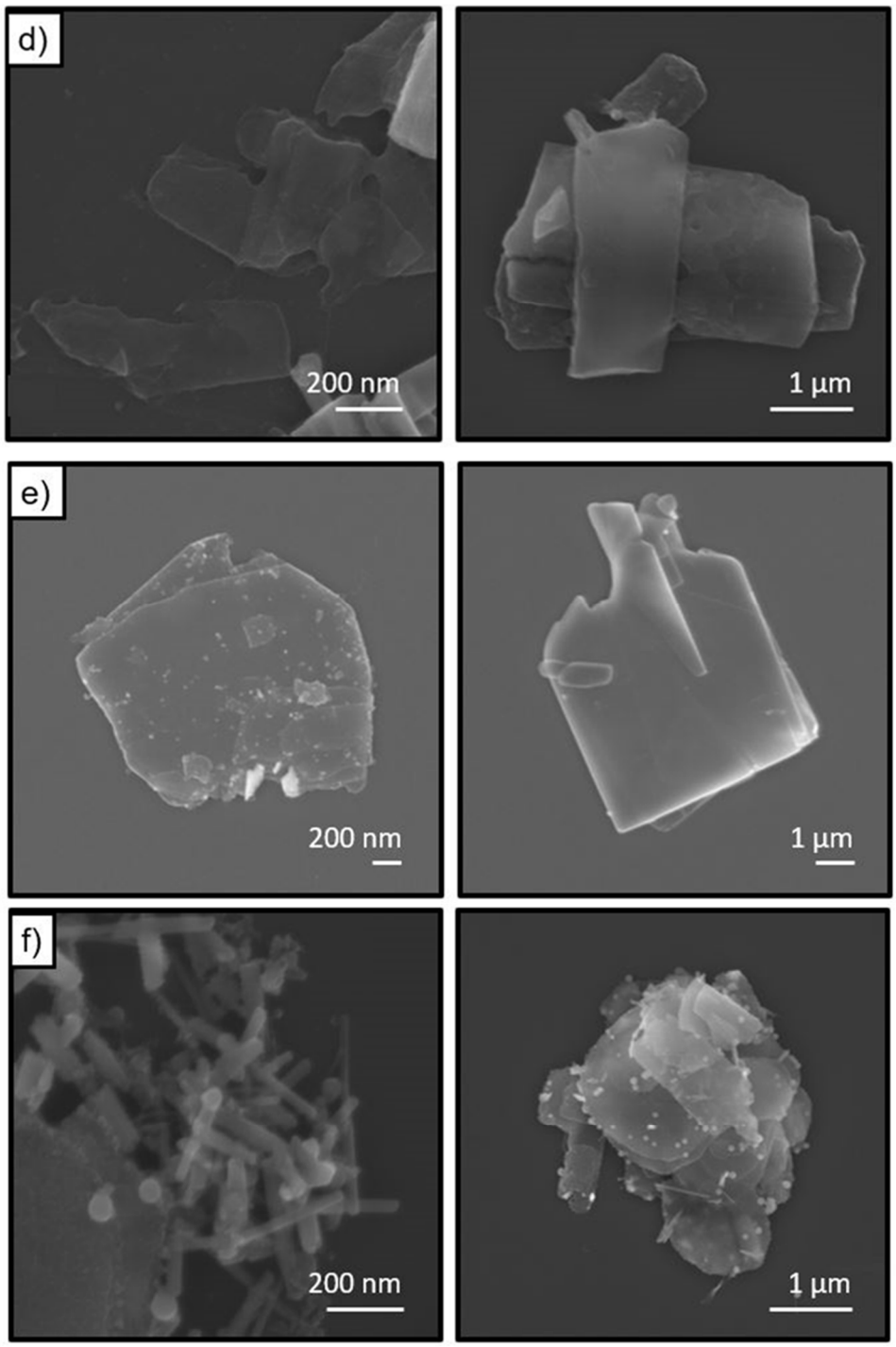

Figure S10. SEM images of ZnSe(ba) exfoliated from different solvents. a) EtOH; b) THF; c) DMF; d) NMP; e) ethylene glycol; f) H_2O. Two representative images are provided for each sample.

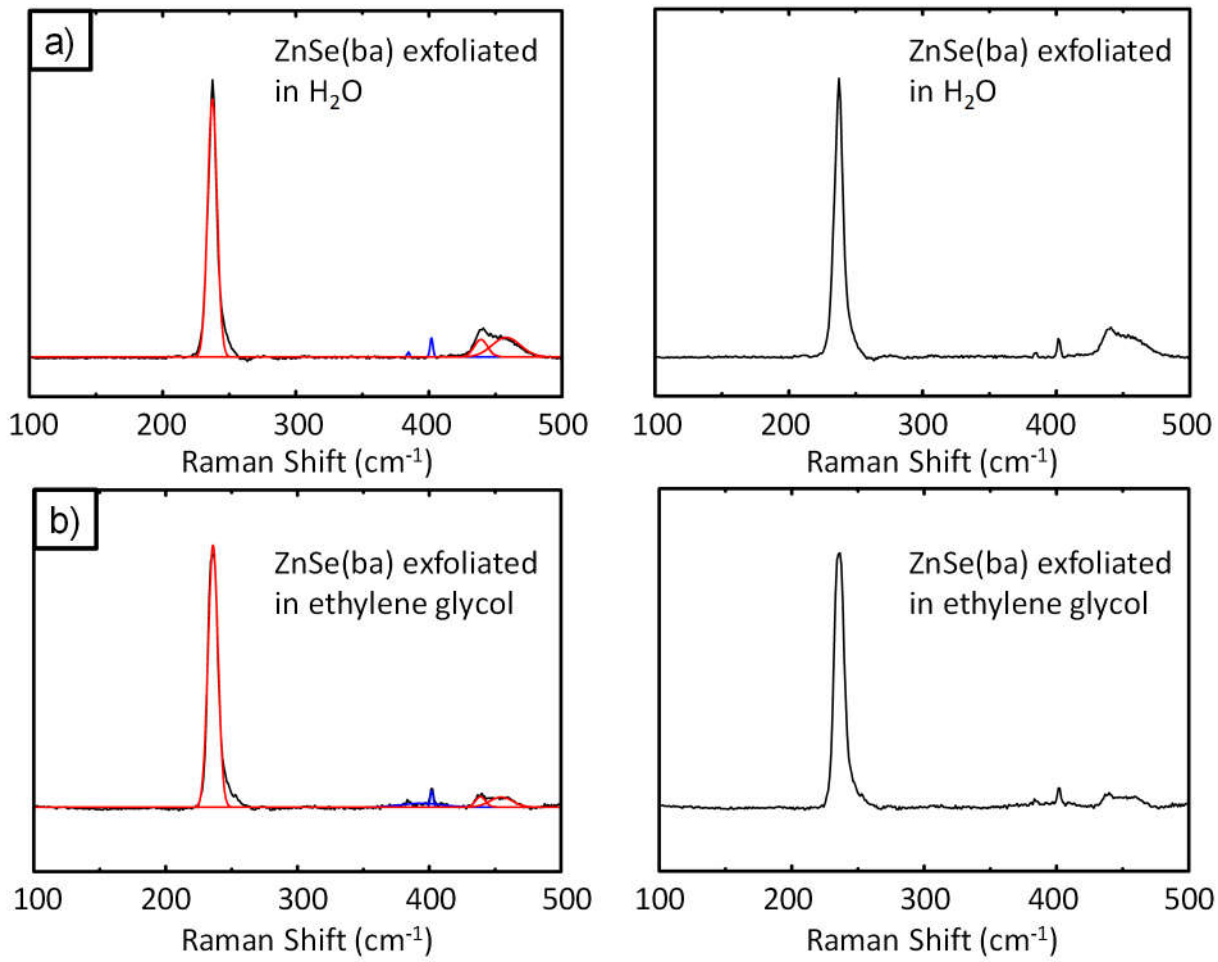

Figure S11. Raman spectra with (left) and without (right) peak fitting of ZnSe(ba) exfoliated from a) H_2O and b) ethylene glycol. Red peaks centered at 236 cm^{-1}, 439 cm^{-1}, and 458 cm^{-1} correspond to Raman shifts characteristic of h-Se nanowires. Blue peaks at 385 cm^{-1} and 402 cm^{-1} originate from native ZnSe(ba).

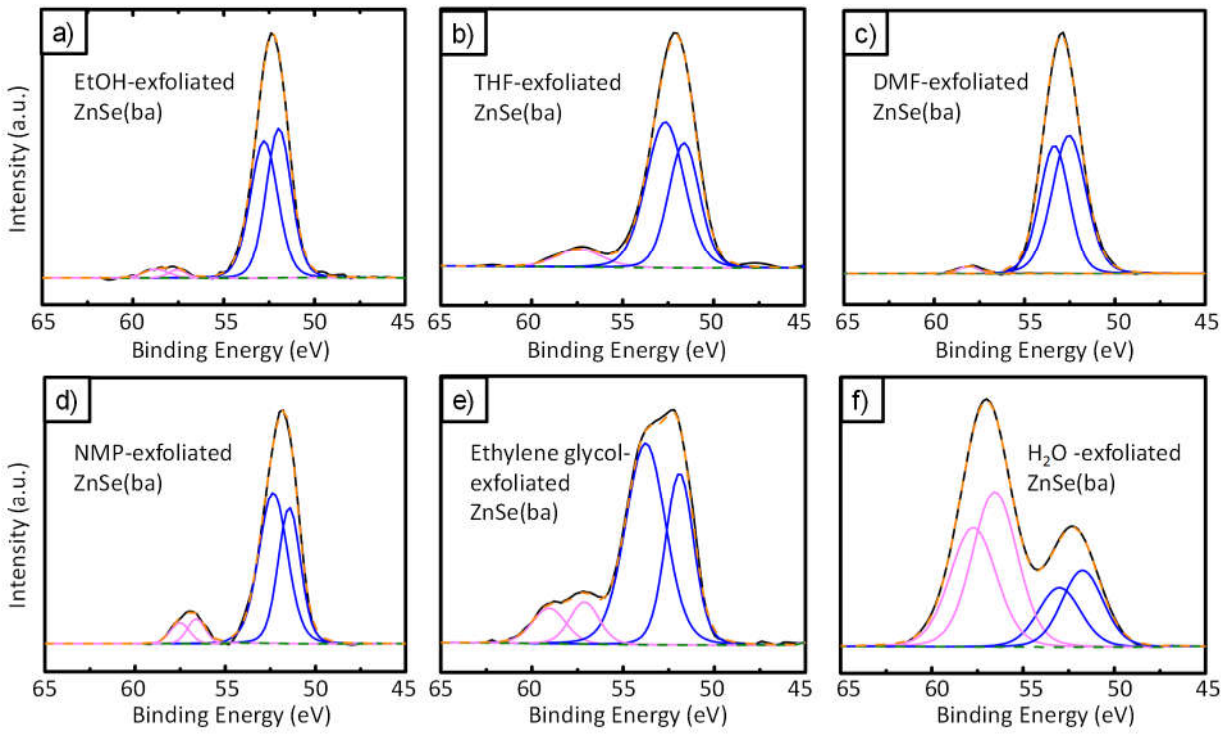

Figure S12. X-ray photoelectron spectra of ZnSe(ba) exfoliated at 6000 rpm for 1 h from a) EtOH, b) THF, c) DMF, d) NMP, e) ethylene glycol and f) H_2O. Black lines indicate experimental data, dashed olive lines indicate fitted Shirley[4] backgrounds, dashed orange lines indicate fitting envelopes, and blue and pink lines correspond to signals measured experimentally for ZnSe and Se, respectively. The integrated peak intensity ratios of ZnSe:Se are summarized in Table S2. All samples were measured 11 days after exfoliation. All samples were stored in their respective exfoliation solvents at room temperature without further handling (drying) until the day before analysis. Samples were dried under reduced pressure (~1 Torr) for 24 h prior to analysis.

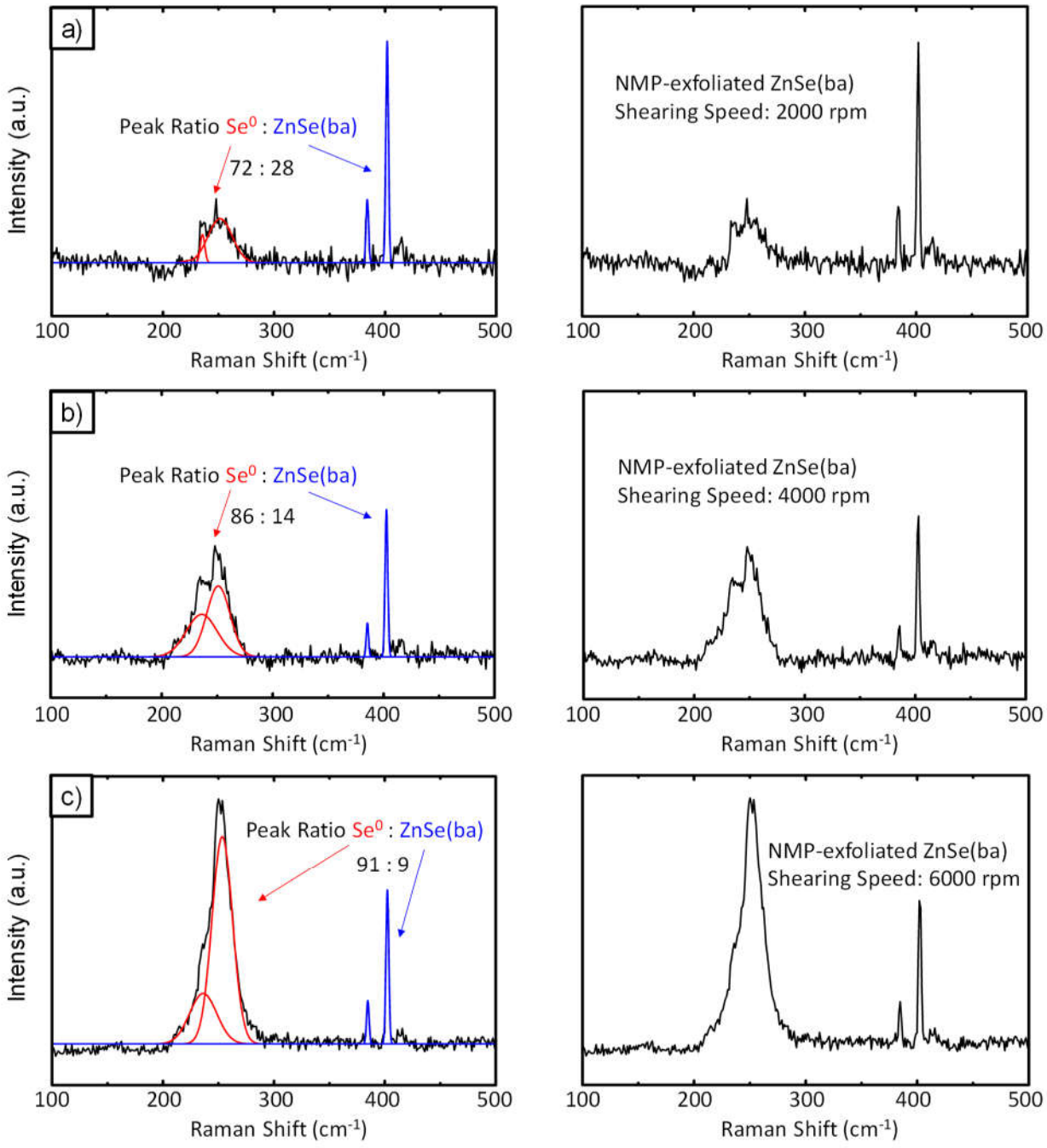
a)
Peak Ratio Se0 : ZnSe(ba)
72 : 28
Intensity (a.u.)
Raman Shift (cm-1)
NMP-exfoliated ZnSe(ba)
Shearing Speed: 2000 rpm
b)
Peak Ratio Se0 : ZnSe(ba)
86 : 14
NMP-exfoliated ZnSe(ba)
Shearing Speed: 4000 rpm
c)
Peak Ratio Se0 : ZnSe(ba)
91 : 9
NMP-exfoliated ZnSe(ba)
Shearing Speed: 6000 rpm
100
200
300
400
500

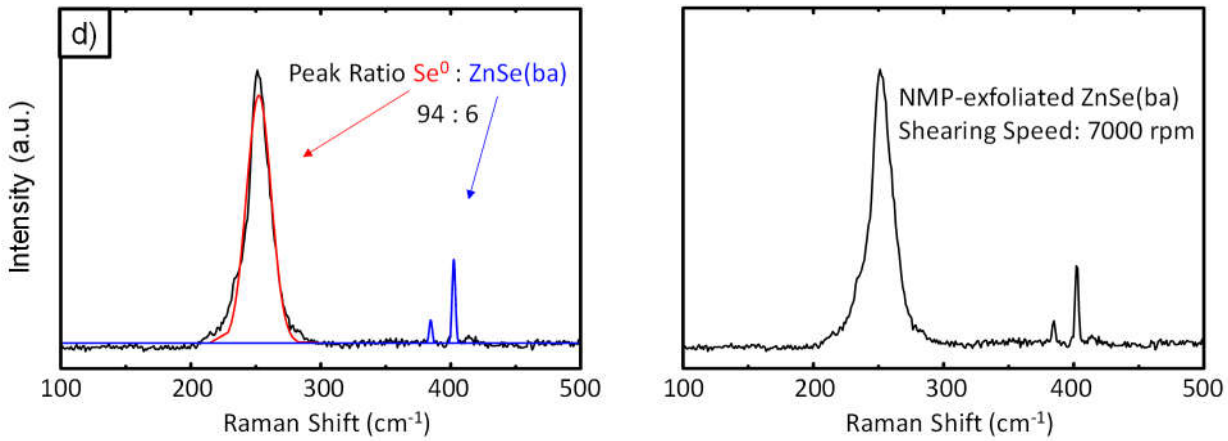

Figure S13. Raman spectroscopic analysis of NMP-exfoliated ZnSe(ba) at different shear speeds. The red peak fits indicate the presence of amorphous Se and h-Se nanowires (labeled as Se^0).[5] The blue peak fits originate from ZnSe(ba). The ratio of integrated intensities of the red and blue peaks is indicated in the left panel of each figure. the right panel of each figure shows the original baseline-subtracted Raman spectrum (without peak fits shown).

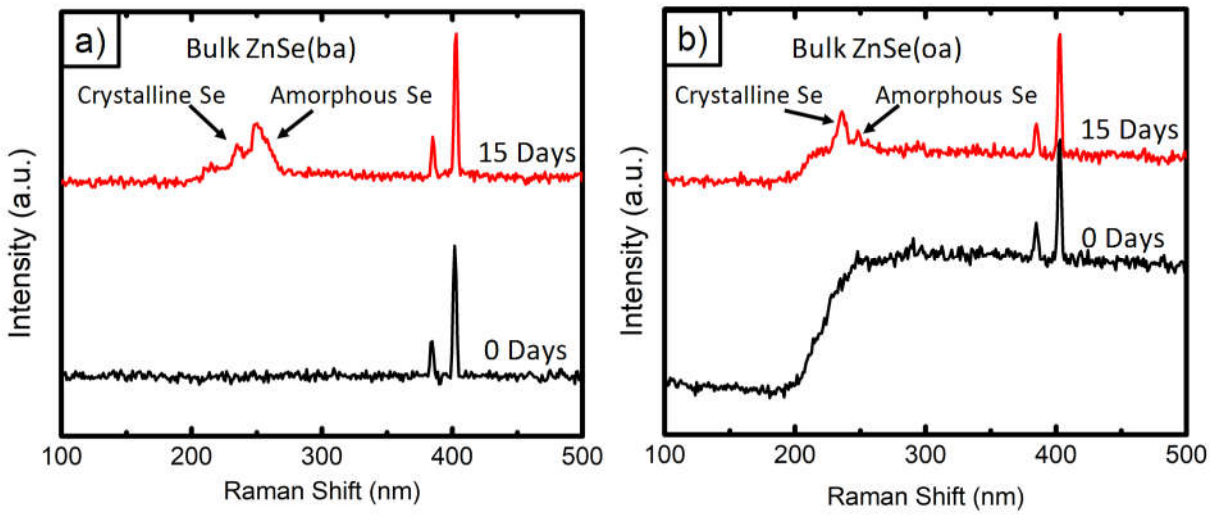

Figure S14. Raman spectra of dry, bulk ZnSe(ba) and ZnSe(oa) powders left in ambient conditions for 0 and 15 days.

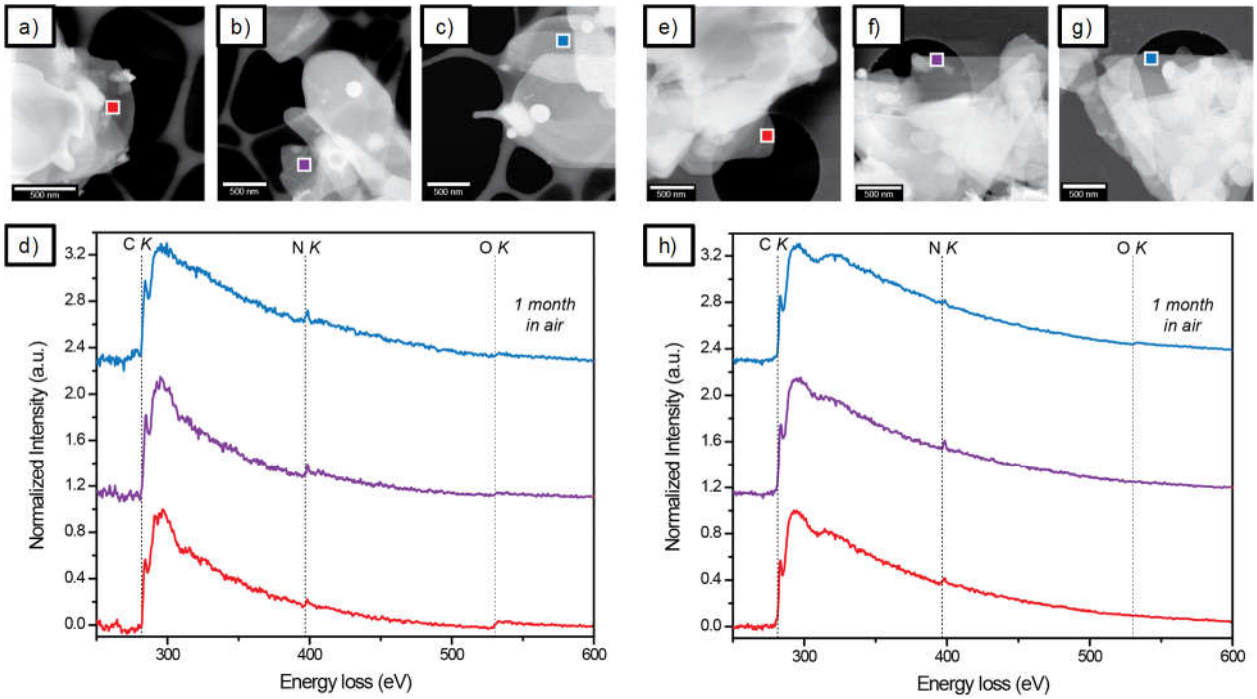

Figure S15. a-c) ADF-STEM images of three flakes of ZnSe(ba) exfoliated in EtOH and d) corresponding EELS spectra at the C, N, and O K ionization edges. e-g) ADF-STEM of three flakes of ZnSe(oa) exfoliated in EtOH and h) corresponding EELS spectra at the C, N, and O K ionization edges. Colored squares mark the location of the spectra and are matched in color with the line colors for the spectra. The spectra for samples shown in (a), (b), (e) and (f) were recorded after 20 days for (a) and (b), and 14 days for (e) and (f), following exfoliation. Samples were stored in an oxygen- and moisture-free environment before characterization. The spectra from the samples shown in (c) and (g) were recorded after storing the samples for 1 month in ambient conditions.

Figure S15a-d presents EELS data on ZnSe(ba) exfoliated in EtOH. The intensity recorded at the O *K* edge varied between samples shown in Figures S15a and S15b, indicating the degree of oxidation was inhomogeneous throughout the sample. Following a month in air, flakes were found with comparable degrees of oxidation with signal at the N *K* edge still present. Different flakes were selected for analysis to avoid uncertainties associated with electron-beam induced sample changes. These data demonstrate that oxidation is present in ZnSe(ba) exfoliated in EtOH immediately after exfoliation. Oxidative degradation is not complete after 1 month.

Figure S15 e-h presents EELS data on ZnSe(oa) exfoliated in EtOH. The relative C *K* intensity is greater for all ZnSe(oa) samples relative to the ZnSe(ba) samples, consistent with the longer alkyl chain. No intensity was recorded at the O *K* edge for samples shown in Figures S15e and S15f, indicating no oxidation of the ZnSe(oa) at the limit of detection. Following a month in air, no flakes without

intensity at the O *K* edge were identified. Flakes were found with measurable intensity at the O *K* edge though intensity at the N *K* edge was also still present. Different flakes were selected for analysis to avoid uncertainties associated with electron-beam induced sample changes. These data demonstrate that negligible oxidation is present in ZnSe(oa) exfoliated in EtOH immediately after exfoliation. No sample material exhibiting undetectable oxidation was found after 1 month in air. Oxidative degradation is not complete after 1 month.

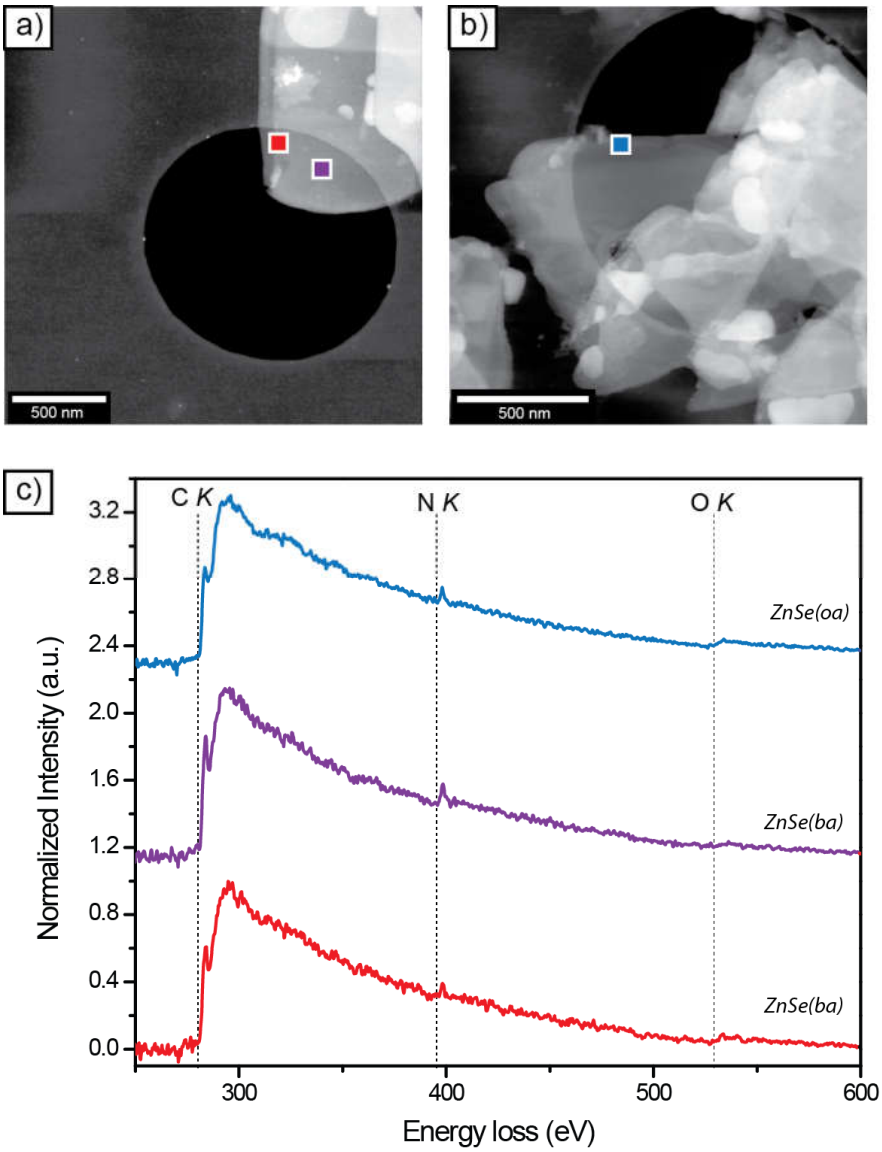

Figure S16. ADF-STEM of (a) ZnSe(ba) and b) ZnSe(oa) exfoliated in NMP and c) corresponding EELS at the C, N, and O *K* ionization edges. Colored squares mark the location of the spectra and are matched in color with the line colors for the spectra. Spectra were recorded <20 days after exfoliation.

Figure S16 presents EELS data on ZnSe(ba) and ZnSe(oa) exfoliated in NMP. Intensity was recorded at the O *K* edge for both samples shown, indicating detectable oxidation shortly after exfoliation. Intensity at the N *K* edge was also still present. Increased O *K* intensity was recorded for positions near a flake edge (higher O *K* signal in red, lower O *K* signal in purple). This spatial variation was analyzed further by independent component analysis (ICA) presented in Figures S17 and S18.

These data demonstrate that oxidation occurs in NMP exfoliated ZnSe(alkylamine) regardless of ligand selection.

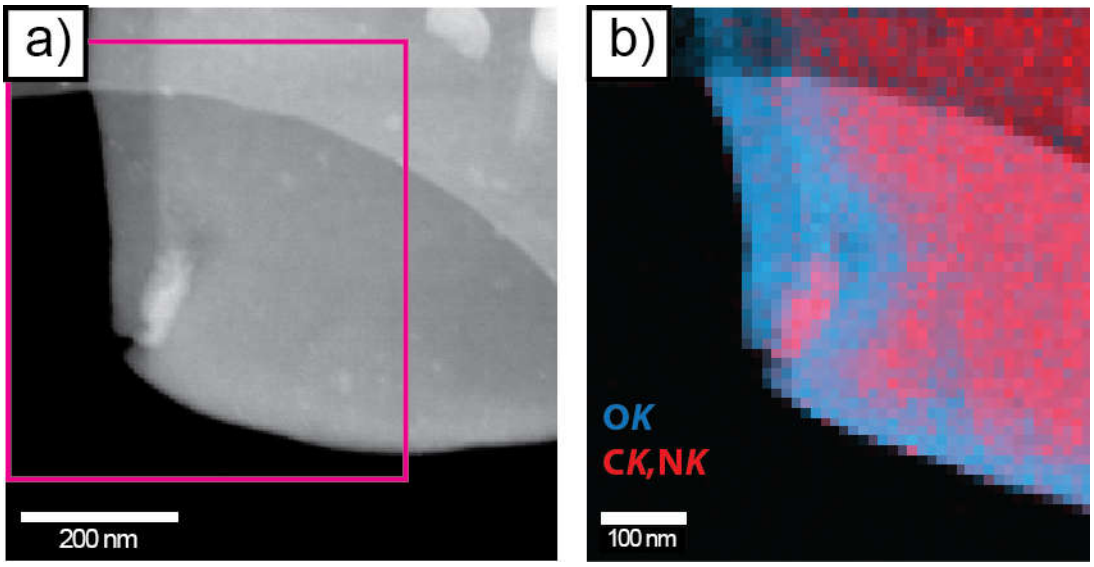

Figure S17. a) ADF-STEM and b) ICA loading map composite extracted from EELS at the C, N, and O *K* ionization edges for a flake of ZnSe(ba) exfoliated in NMP. The pink rectangle in a) marks the location of EELS spectrum image. The signature associated with O is shown in blue and the signature associated with C and N is shown in red.

Hyperspectral data sets consisting of individual spectra recorded at each probe position in a microscopic field of view contain highly redundant information and are therefore highly suited for machine learning based techniques for data analysis. ICA has been demonstrated to separate chemically distinct EELS features to map spatially varying composition and oxidation state.[6-7] In brief, ICA is a type of blind source separation using statistical analysis to un-mix a data-set into its constituent spectral components and corresponding loading maps which reflect the weight of each component at each pixel in an image or, equivalently, each probe position in STEM-EELS. The ICA algorithm identifies maximally independent spectral components based on the variance characteristics in the data set.

Figure S17 presents two ICA loading maps corresponding to a predominant O *K* edge feature (blue) and a second feature (red) consisting of the characteristic C *K* and N *K* near edge fine structure for ZnSe(ba). The full set of loading maps and corresponding spectral components are shown for reference in Figure S18.

The loading maps in Figure S17 reflect the spatial distribution of oxidation and pristine ZnSe(ba). The blue intensity is maximal at the edge, indicating enhanced oxidation at the flake edge. This observation is consistent with the selected area spectra shown in Figure S17. Additionally, the width of the region at the edge showing enhanced oxidation is approximately 40-50 nm along the lower edge. Areas with a stepped multi-edge thickness variation recorded in ADF-STEM (left edge)

show a wider oxidized edge layer. This 40-50 nm wide edge region is the same size as regions showing loss of crystallinity (Figures S15, S19, and S20).

These data demonstrate correlated chemical and structural degradation at the edges of exfoliated ZnSe(alkylamine) flakes.

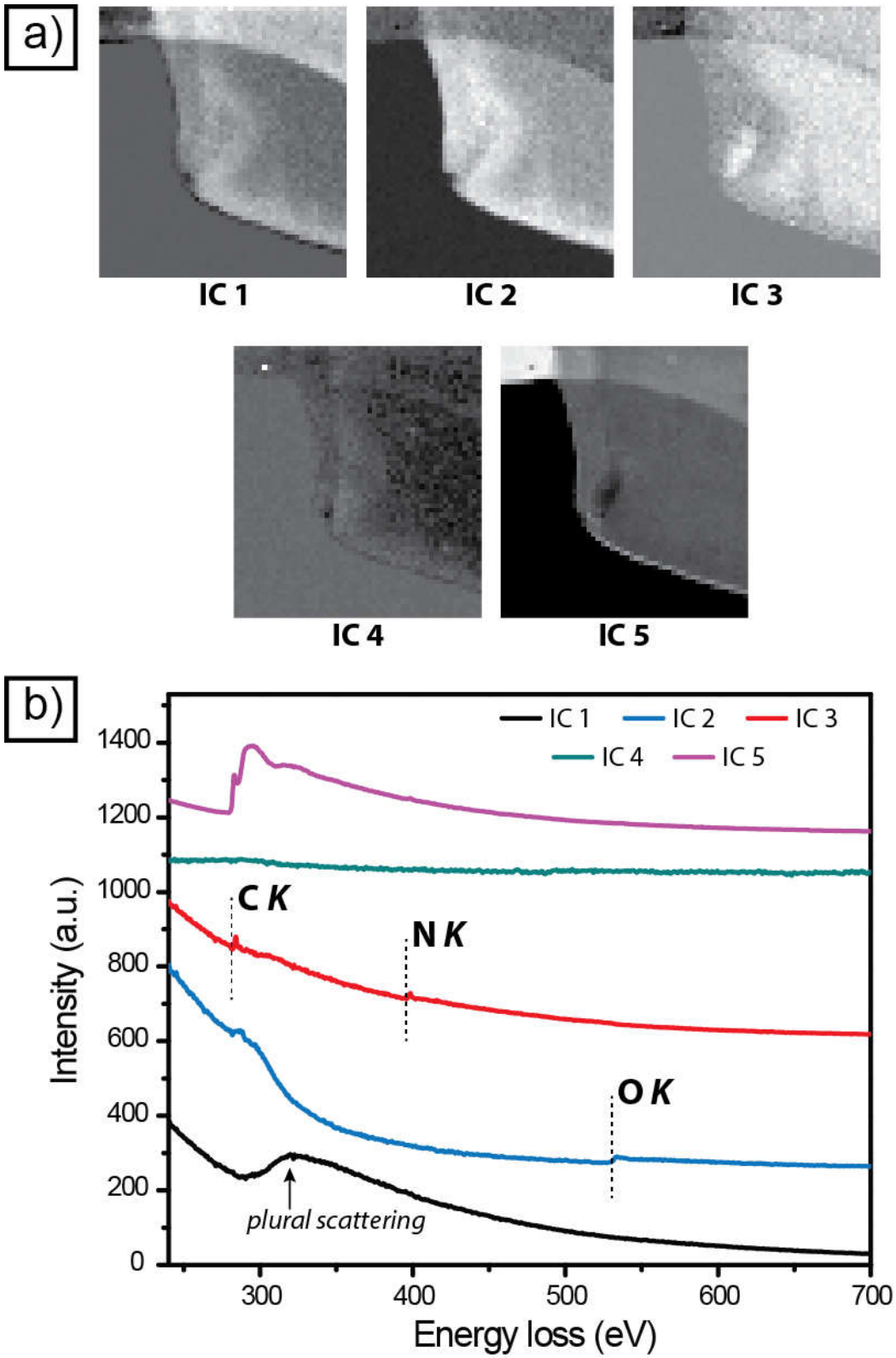

Figure S18. a) ICA loading maps and b) corresponding spectral factors for all five independent components retrieved from the EELS data set.

Figure S18 presents the complete ICA results for the EELS data set depicted in Figure S17. The number of components was determined from a preliminary singular value decomposition, directly related to principal component analysis.[8] A scree plot was used to judge the number of components required to describe the data set. In Figure S18, the first component (IC 1) shows the characteristic signature of plural scattering EELS, that is multiple inelastic scattering arising from electron undergoing both C *K* ionization and plasmon scattering giving rise to a maximum shifted by the plasmon energy approximately 20-30 eV beyond the C *K* ionization edge. IC 2 is the only component showing intensity at the O *K* edge. IC 3 captures the fine structure for ZnSe(ba) at the C and N *K* ionization edges, attributed to pristine ZnSe(ba). IC 4 did not show significant spectral features and was attributed to detector offset. IC 5 shows a characteristic fine structure of amorphous carbon and was attributed to the support film, consistent with the observed spatial variation showing intensity following the contour of the hole in the carbon support film.

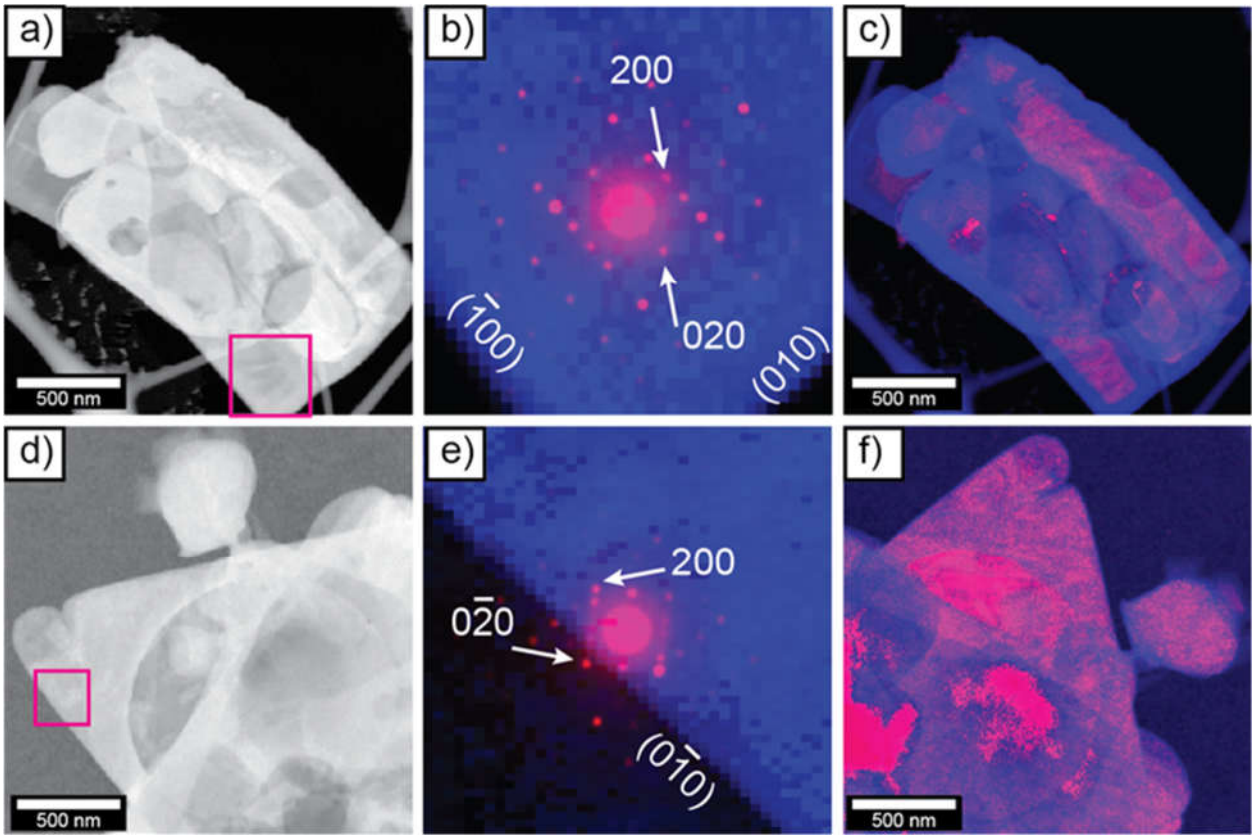

Figure S19. A second example of SED analysis of a)-c) ZnSe(ba) and d)-f) ZnSe(oa) exfoliated in EtOH. a), d) Dark field micrographs obtained by integration of scattering intensity. b), e) Overlays of images (blue) and diffraction patterns (magenta) for selected regions marked in a), d). The poles are marked with arrows on the diffraction patterns and the corresponding surface planes are labeled on the images. c), f) Overlays of images (blue) and crystallinity maps (magenta) formed by counting the Bragg peaks in diffraction patterns at each probe position.

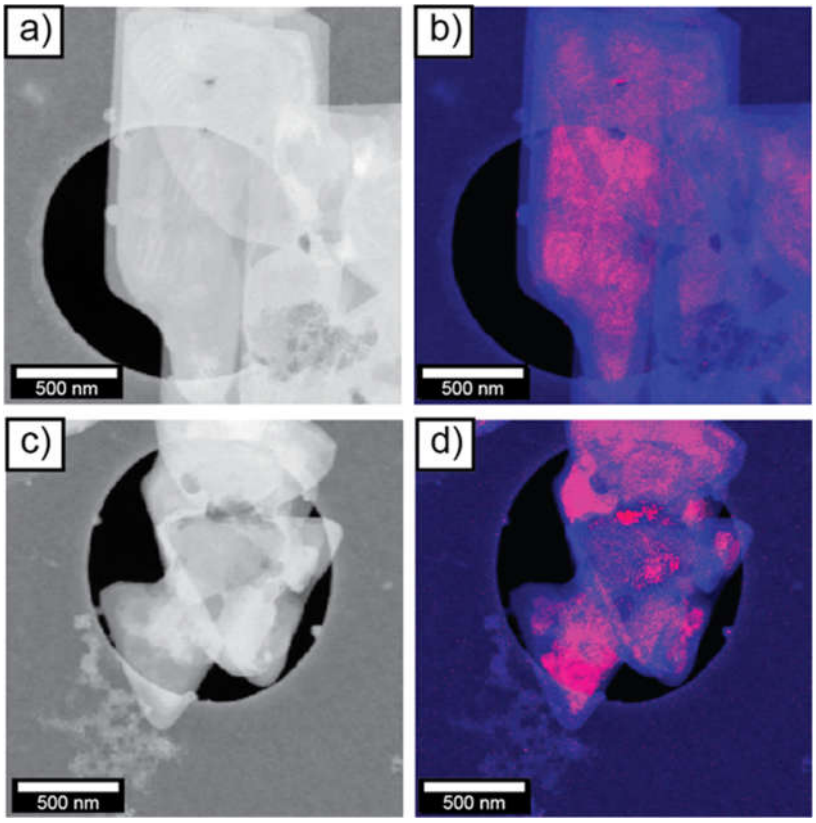

Figure S20. SED analysis of a)-b) ZnSe(ba) and c)-d) ZnSe(oa) exfoliated in NMP. a), c) Dark field micrographs obtained by integration of scattering intensity. b), d) Overlays of images (blue) and crystallinity maps (magenta) formed by counting the Bragg peaks in diffraction patterns at each probe position.

Shearing conditions: 6000 rpm, 1h	Dispersion concentration (g/L)			
Solvent	Trial 1	Trial 2	Trial 3	Averaged Conc.
EtOH	0.015	0.011	0.019	0.015 ± 0.003
THF	0.000	0.000	0.000	N/A
DMF	0.031	0.027	0.034	0.03 ± 0.002
NMP	0.021	0.020	0.025	0.022 ± 0.002
Ethylene glycol	0.049	0.035	0.052	0.045 ± 0.007
H_2O	0.013	0.012	0.015	0.013 ± 0.001

Table S1. Concentrations of ZnSe(ba) exfoliated in different solvents after shear mixing at 6000 rpm for 1 h, followed by centrifugation at 1500 rpm for 40 min.

Shearing conditions: 6000 rpm, 1h	Sample Used: ZnSe(ba)
Solvent	Extent of Oxidation (% ZnSe:% Se)
EtOH	92.4 : 7.2
THF	92.0 : 8.0
DMF	95.4 : 4.6
NMP	88.8 : 11.2
Ethylene glycol	84.4 : 15.6
H_2O	28.0 : 72.0

Table S2. Oxidation rate of ZnSe(ba) after shear exfoliation in different solvents, measured by XPS. A lower ratio of ZnSe:Se indicates a greater extent of oxidation.

References.

1. Stokes, G. G., *On the Effect of the Internal Friction of Fluids on the Motion of Pendulums*. Pitt Press Cambridge, 1851; Vol. 9.
2. Egerton, R. F., *Electron Energy-Loss Spectroscopy in the Electron Microscope*. 3rd ed.; Springer: New York, 2011.
3. Iakoubovskii, K.; Mitsuishi, K.; Nakayama, Y.; Furuya, K. Thickness Measurements with Electron Energy Loss Spectroscopy. *Microsc. Res. Tech.* ***2008***, ***71*** (8), 626-631.
4. Shirley, D. A. High-Resolution X-Ray Photoemission Spectrum of the Valence Bands of Gold. *Phys. Rev. B* ***1972***, ***5*** (12), 4709-4714.
5. Ren, L.; Zhang, H.; Tan, P.; Chen, Y.; Zhang, Z.; Chang, Y.; Xu, J.; Yang, F.; Yu, D. Hexagonal Selenium Nanowires Synthesized via Vapor-Phase Growth. *J. Phys. Chem. B* ***2004***, ***108*** (15), 4627-4630.
6. de la Peña, F.; Berger, M. H.; Hochepied, J. F.; Dynys, F.; Stephan, O.; Walls, M. Mapping Titanium and Tin Oxide Phases Using EELS: An Application of Independent Component Analysis. *Ultramicroscopy* ***2011***, ***111*** (2), 169-176.
7. Collins, S. M.; Fernandez-Garcia, S.; Calvino, J. J.; Midgley, P. A. Sub-Nanometer Surface Chemistry and Orbital Hybridization in Lanthanum-Doped Ceria Nano-Catalysts Revealed by 3D Electron Microscopy. *Sci. Rep.* ***2017***, ***7*** (1), 5406.
8. Shlens, J. A Tutorial on Principal Component Analysis. *arXiv preprint arXiv:1404.1100* ***2014***.